2-3-2015

# Coordinated investigation of mid-latitude upper mesospheric temperature inversion layers and the associated gravity wave forcing by Na lidar and Advanced Mesospheric Temperature Mapper at Logan, Utah (42°N)

Tao Yuan
*Utah State University*, titus.yuan@usu.edu

Pierre-Dominique Pautet
*Utah State University*, dominiquepautet@gmail.com

Yucheng Zhao
*Utah State University*, yu.cheng@usu.edu

Xuguang Cai
*Utah State University*

Neal R. Criddle
*Utah State University*, neal.criddle@aggiemail.usu.edu

Michael J. Taylor
*Utah State University*, mike.taylor@usu.edu



## Recommended Citation

*See next page for additional authors*

Yuan T., Pautet P.-D., Zhao Y., Cai X., and Taylor M.J., Coordinated investigation of mid-latitude upper mesospheric temperature inversion layers and the associated gravity wave forcing by Na lidar and Advanced Mesospheric Temperature Mapper at Logan, Utah (42°N), J. Geophys. Res., 119 (7), 3756-3769, 2014

AGU PUBLICATIONS

JGR

Journal of Geophysical Research: Atmospheres

RESEARCH ARTICLE
10.1002/2013JD020586

**Key Points:**
- The mesospheric temperature inversion is formed by gravity wave breaking
- The wave breaking due to enhanced saturation and statically unstable region
- Tidal wave and mesospheric bore induce sharp increase of stability

**Correspondence to:**
T. Yuan,
titus.yuan@usu.edu

**Citation:**
Yuan, T., P.-D. Pautet, Y. Zhao, X. Cai, N. R. Criddle, M. J. Taylor, and W. R. Pendleton Jr. (2014), Coordinated investigation of midlatitude upper mesospheric temperature inversion layers and the associated gravity wave forcing by Na lidar and Advanced Mesospheric Temperature Mapper in Logan, Utah, *J. Geophys. Res. Atmos.*, *119*, 3756–3769, doi:10.1002/2013JD020586.

Received 18 JUL 2013
Accepted 13 MAR 2014
Accepted article online 14 MAR 2014
Published online 7 APR 2014

# Coordinated investigation of midlatitude upper mesospheric temperature inversion layers and the associated gravity wave forcing by Na lidar and Advanced Mesospheric Temperature Mapper in Logan, Utah

**Tao Yuan[1], P.-D. Pautet[1], Y. Zhao[1], X. Cai[2], N. R. Criddle[2], M. J. Taylor[1,2], and W. R. Pendleton Jr.[1]**

[1]Center for Atmospheric and Space Sciences, Utah State University, Logan, Utah, USA, [2]Department of Physics, Utah State University, Logan, Utah, USA

**Abstract** Mesospheric inversion layers (MIL) are well studied in the literature but their relationship to the dynamic feature associated with the breaking of atmospheric waves in the mesosphere/lower thermosphere (MLT) region are not well understood. Two strong MIL events ($\Delta T$ ~30 K) were observed above 90 km during a 6 day full diurnal cycle Na lidar campaign conducted from 6 August to 13 August Logan, Utah (42°N, 112°W). Colocated Advanced Mesospheric Temperature Mapper observations provided key information on concurrent gravity wave (GW) events and their characteristics during the nighttime observations. The study found both MILs were well correlated with the development and presence of an unstable region ~2 km above the MIL peak altitudes and a highly stable region below, implicating the strengthening of MIL is likely due to the increase of downward heat flux by the enhanced saturation of gravity wave, when it propagates through a highly stable layer. Each MIL event also exhibited distinct features: one showed a downward progression most likely due to tidal-GW interaction, while the peak height of the other event remained constant. During further investigation of atmospheric stability surrounding the MIL structure, lidar measurements indicate a sharp enhancement of the convective stability below the peak altitude of each MIL. We postulate that the sources of these stable layers were different; one was potentially triggered by concurrent large tidal wave activity and the other during the passage of a strong mesospheric bore.

## 1. Introduction

Lidars have been observing and investigating the mesospheric inversion layer (MIL), a transient temperature anomaly, within the mesosphere and lower thermosphere for a couple of decades [*Hauchecorne et al*., 1987; *Dao et al*., 1995; *Meriwether et al*., 1998]. The inversion layers are regions of temperature enhancements with amplitudes that can reach 20–30 K or even larger. Most of the reports are characterized by downward propagation of 1–3 km/h, which falls well within the range of tidal waves vertical phase speed. Such temperature inversion layers are believed to be formed by atmospheric gravity wave (GW)-mean flow interaction and/or wave-wave interactions occurring within the upper atmosphere. *Meriwether and Gerrard* [2003] gave a comprehensive review of this phenomenon and summarized that although other mechanisms may exist for the formation of MIL, such as chemical heating [*Meriwether and Mlynczak*, 1995; *States and Gardner*, 2000], there are two major types of MIL events. The first one is found to be mostly formed near 60–70 km altitude and has been consistently observed by Rayleigh lidar around the globe during the Northern Hemisphere winter near middle and high latitudes [*Hauchecorne et al*., 1987; *Cutler et al*., 2001; *Duck et al*., 2001]. The other one occurs at higher altitude around 90 km and is often detected by Na lidar [*Meriwether et al*., 1998; *Huang et al*., 1998]. Various modeling studies coupled with satellite measurements have shown that "lower" MILs observed at midlatitudes during winter are due to planetary wave interaction at a critical level, which is related to GW breaking in the mesosphere. Such interactions form a compact "mesospheric surf zone" and induce lower MILs [*Sassi et al*., 2002; *Oberheide et al*., 2006] that can last for days in the mesosphere. On the other hand, *Sica et al*. [2007] concluded that, depending on the combination of the atmospheric background lapse rate and the magnitude of the wave modulation, any breaking atmospheric wave could trigger a MIL. This latter theory is in agreement with their multiyear Rayleigh lidar observations at the University of Western Ontario. "Upper" MILs are more transient events and happen mostly near 90 km where the tidal amplitude

becomes significant. Since their altitudes are near the peak of the mesospheric Na layer, a Na lidar therefore generates the best signal-to-noise (S/N) data and is an ideal instrument for studying this topic. Lidar observations indicate upper MILs are most likely generated through tidal-GW interactions [*Meriwether and Gardner*, 2000; *States and Gardner*, 2000; *Sica et al*., 2002], thus exhibiting a downward phase progression, similar to the tidal wave vertical wavelength. *Liu and Hagan* [1998] showed in their model study that during the breaking of upward propagating GWs, the amplitude of the horizontal advection of potential temperature decreases much slower than that of the vertical advection, causing net cooling within the breaking region. Since the breaking region is confined by GW critical level, which is modulated by the tidal wind, the downward phase progression of the tidal wave guides the unstable (cooling) region downward with a descent rate related to both the tidal wave vertical phase speed and the descent rate of GW breaking level. During this process, the simultaneous increase of the downward heat flux due to enhanced eddy diffusion causes temperature enhancement below the cooling region and forms a temperature inversion layer, which carries GW and tidal phase information. *Liu et al*. [2000] further studied tidal wave modulation of this GW-mean flow interaction by using a two-dimensional model that indeed duplicated the downward progress of critical level and the associated upper MIL. *Huang et al*. [1998] conducted a detailed study of mesopause region during an upper MIL event using Na lidar observations during the 1993 Airborne Lidar and Observations of the Hawaiian Airglow (ALOHA-93) campaign, confirming the amplitude of the layer is associated with energy deposition resulting from GW/critical level interaction. However, without high-resolution diurnal cycle temperature and horizontal wind observations, it is difficult to distinguish the abnormal upper MILs from the temperature maximum induced by the tidal modulation. In addition, simultaneous 24 h continuous horizontal wind measurements are essential for quantifying the GW critical level behavior relative to the tidal wind field. Such observations in the MLT region are rare, and experimental investigations on this topic are important for the development of the associated theory and modeling studies.

The Utah State University (USU) Na lidar system (42°N, 112°W), which was relocated from its original operational site at Colorado State University (CSU) (41°N, 105°W) in summer 2010, has the capability to run full diurnal cycle observations of mesopause region temperature and horizontal winds. These diurnal cycle observations can be used to deduce tidal perturbations and variability for various studies. We have established tidal climatology based on multiyear lidar measurements [*Yuan et al*., 2006, 2008a, 2010], which can provide the guide of tidal wave behavior for the USU lidar measurements. In addition to these capabilities, the nighttime coplanar lidar beam setup allows the measurements of the GW momentum flux [*Acott et al*., 2011] that is directly related to GW forcing and is essential to study the GW-mean flow interactions. The surrounding upper atmospheric remote sensing instruments at USU can give a much more comprehensive picture of GWs, tidal waves, planetary waves, and mean field information during the lidar campaign. For example, the colocated Advanced Mesospheric Temperature Mapper (AMTM) provides key measurements of small-scale GWs, such as their propagating directions and horizontal phase speeds, and the Meteor Wind Radar located at the nearby Bear Lake Observatory provides characteristics of planetary wave behavior through its continuous zonal and meridional wind observations.

In this paper, we investigate two upper MIL events captured during one of these multi-instrument summer campaign conducted from 6 to 13 August 2011 (UT day 218 to 225). (To be succinct, we will omit the term upper for the rest of the paper.) During the campaign, two strong MIL events were observed by the lidar on the nights of day 221 and day 223, both of which lasted more than 2 h and exhibited pronounced crest-to-trough temperature perturbation $>$30 K. The lidar was set up to measure the GW zonal momentum flux, the temperature, horizontal wind, and atmospheric stability changes during these MIL events. These critical dynamic parameters, which are related to MIL formation and propagation, can be utilized to have a comprehensive investigation on this temperature anomaly during this type of joint campaign that involves a cluster of instruments. Specifically, the analysis of these results has helped reveal the connection between the variations of the small-scale, short-period GWs and the large-scale modulations, such as tidal and planetary waves.

The layout for the rest of this paper is as follows: description of the instruments involved in the campaign is in section 2, followed by the MIL observations by the Na lidar in section 3 which includes lidar-measured zonal momentum flux and atmospheric instability assisted by GW measurements using the AMTM. Detailed discussions of these observations and a review some related important GW breaking theories are given in section 4 to facilitate our understanding of the observations. Summary and conclusions are in section 5.

## 2. Instruments

The Na lidar system is a narrowband resonance fluorescence Doppler lidar system operating at the Na $D_2$ line with a 120 MHz full width at half maximum (FWHM) laser pulse bandwidth. It is the heritage of the Na lidar system developed at Colorado State University (CSU), which was relocated to USU in the summer of 2010, after two decades of operations in Colorado. It provides critical atmospheric information such as temperature, Na density, zonal, and meridional wind profiles throughout a full diurnal cycle of observations of the mesopause region (80–110 km). The Na lidar is currently set up to probe the mesopause region in three directions (north, east, and west) during the night and in two directions (north and east) during the daytime operations by using a pair of Faraday filters to strongly reject the sky background. The lidar operated for 128 h from 04:15 UT on day 218 to 18:12 UT on day 225 with a data gap between 12:00 UT on day 218 and 18:50 UT on day 220, due to adverse weather conditions. Such diurnal cycle lidar observations have proven to be essential for studying variations in the mean fields and tidal waves (24, 12, 8, and 6 h) [*She et al*., 2004], and for establishing climatologies [*Yuan et al*., 2006, 2008a, 2008b, 2010] for the midlatitude mesopause region.

In this paper, different spatial and temporal resolutions are utilized to process lidar data so that GW-induced perturbations or turbulence can be studied, especially during the nocturnal lidar measurements (where 10 min temporal and 2 km vertical resolutions are applied for nighttime lidar data analysis, while the combination of 30 min and 4 km is used for daytime lidar data). The lower spatial resolution during the daytime was necessary to compensate for the reduced signal to noise (S/N) of the lidar data while operating under sunlit conditions. The nocturnal measurements usually last ~8 h during the summer time, and data with measurement errors due to photon noise $<7$ m/s in line of sight wind and 10 K in temperature are used in the subsequent momentum flux (MF) calculations.

The Utah State University Advanced Mesospheric Temperature Mapper (AMTM) is designed to measure the mesospheric OH (3,1) rotational temperatures over a large area, centered on the zenith. This instrument uses a fast (f:/1) 120° field-of-view telecentric lens system designed and built at the Space Dynamics Laboratory, Logan, Utah. It has three 4" narrowband (2.5–3 nm) filters to measure the $P_1(2)$ and $P_1(4)$ emission lines, and a selected background region, mounted in a computer-controlled filter wheel. The detector comprises an InGaAs camera fitted with a $320 \times 256$ pixel sensor, thermoelectrically cooled to $-50$°C to limit the electronic noise, and controlled through a USB port by a Windows computer. The exposure time for each filter is typically 10 s, giving a temperature measurement for each pixel in the image every ~30 s. This imager can operate under full moon conditions with minimal light contamination. Two of these instruments have been built so far. The first one has operated at the South Pole Station (90°S) since 2010 and the second one at the ALOMAR observatory in Northern Norway (69°N) since the winter 2010–2011. During the summer months, the latter instrument is brought back to Utah and operated on the USU campus alongside the Na lidar. Table 1 lists the summary of the AMTM data during these nights, including the observed GW phase speeds (column 6), observed period (column 7), and event propagation directions relative to North (column 5). The columns 3 and 4 list the start and end of each GW event, respectively, during its observation for every night (column 2).

## 3. Observations of MILs by Na Lidar

Figure 1 shows the Na lidar temperature measurements for the six nights of this collaborated USU campaign in early August (night 218 and nights 221 through 225). During the campaign, the Na lidar was operating in a full diurnal cycle operational mode while the AMTM was operating at night. The diurnal tides have been found quite weak in the midlatitude mesopause region based on various observations and theoretical studies [e.g., *Yuan et al*., 2006, 2010, and references therein], especially during the summer when they reach their minimum. Therefore, diurnal tidal modulation of the temperature during this summer campaign is not expected to be significant. On each temperature contour plot in Figure 1, the established climatological temperature semidiurnal tidal phase profile [*Yuan et al*., 2008a] for August is plotted to locate the temperature maximum induced by the semidiurnal tide so that the MILs can be distinguished from the tidal feature. As shown in the figure, without the guide of the tidal phase profile, temperature features in night 222 (Figure 1, middle left) between 87 km and 94 km before UT 06:30, along with the one in night 224 (Figure 1, bottom left) near the similar altitude and time range can be easily misinterpreted as MILs, while in fact, they are most likely semidiurnal tidal features. The same argument can be applied to the feature in night 221 (Figure 1, top right) between UT 04:30

**Table 1.** Summary of GWs Observed by AMTM During the Campaign in August 2011

| Day # | Time Start | Time Stop | Wavelength (km) ± 3 km | Direction to North (deg) ± 5° | Observed Horizontal Phase Speed (m/s) ± 5 m/s | Observed Period (min) |
|---|---|---|---|---|---|---|
| 218 | 3:57 | 8:01 | 13.4 | 167 | 44.9 | 5.0 |
| | 6:30 | 11:16 | 15.9 | 354 | 57 | 4.6 |
| | 8:40 | 11:16 | 18.8 | 57.5 | 54.7 | 5.7 |
| | 10:10 | 11:16 | 26.2 | 335 | 69.6 | 6.3 |
| 221 | 3:47 | 5:20 | 44.8 | 299 | 44.5 | 16.8 |
| | 4:40 | 8:50 | 20.8 | 45 | 21.9 | 15.8 |
| | 8:10 | 9:20 | 13.2 | 17 | 56.7 | 3.9 |
| | 9:05 | 10:15 | 7.3 | 61 | 62.1 | 2.0 |
| | 9:45 | 10:50 | 12.6 | 11 | 43.9 | 4.8 |
| 222 | 3:45 | 11:20 | 23.7 | 327 | 58.6 | 6.7 |
| | 9:10 | 11:20 | 16.9 | 149 | 10.1 | 27.9 |
| 223 | 3:45 | 11:25 | 20.8 | 332 | 45.2 | 7.7 |
| | 4:00 | 8:00 | 101 | 330 | 37.5 | 45.0 |
| | 3:45 | 6:30 | 19.5 | 197 | 46.3 | 7.0 |
| | 7:50 | 9:10 | 26.7 | 346 | 76 | 5.9 |
| | 8:10 | 11:25 | 15.3 | 17 | 36.2 | 7.0 |
| 224 | 3:40 | 5:10 | 14.2 | 159 | 46.3 | 5.1 |
| | 3:40 | 7:20 | 31.7 | 290 | 79.3 | 6.7 |
| | 6:35 | 7:50 | 9.6 | 333 | 42.4 | 3.8 |
| | 9:40 | 11:25 | 39.7 | 310 | 56.5 | 11.7 |
| 225 | 3:40 | 11:25 | 40.1 | 23 | 31 | 21.6 |
| | 8:20 | 10:25 | 18 | 76 | 27 | 11.1 |

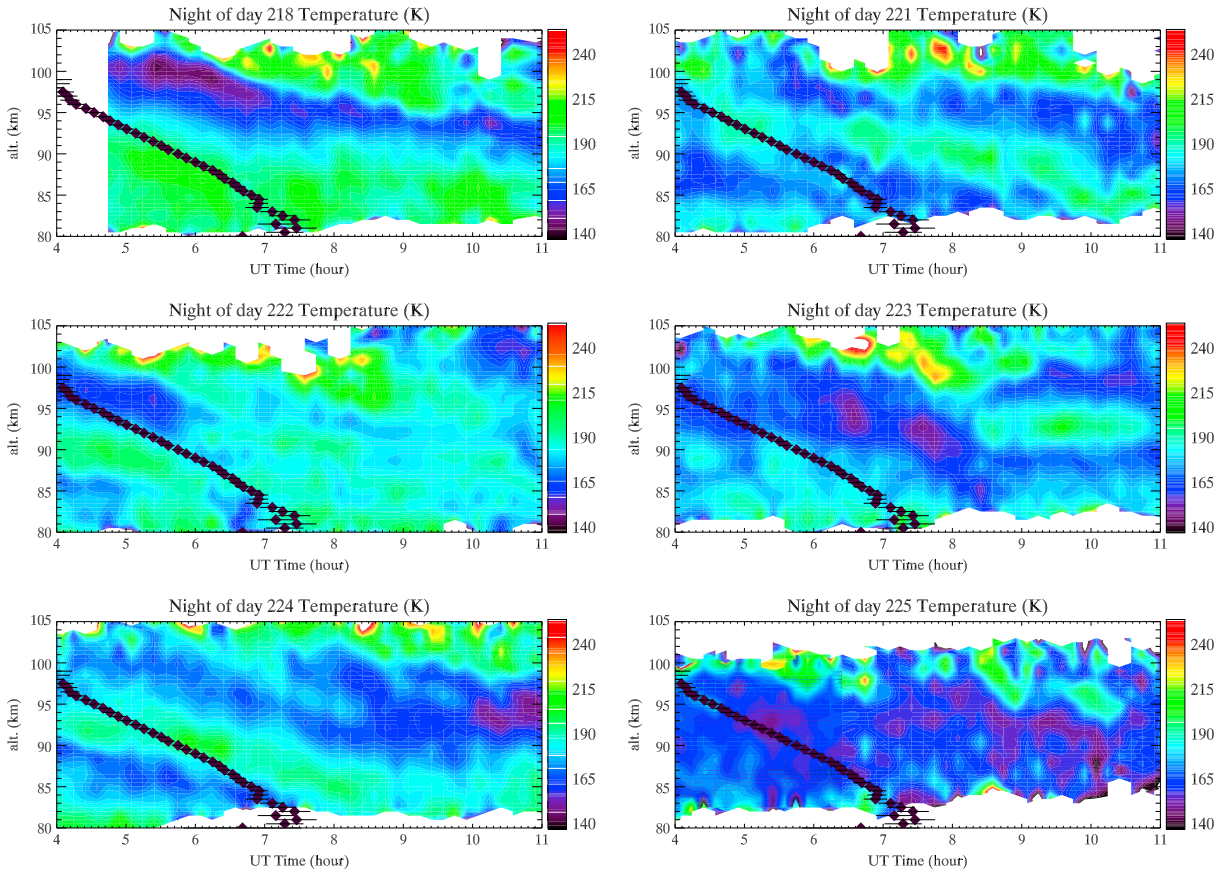


**Figure 1.** Na lidar nocturnal temperature measurements for nights of (top left) day 218, (top right) 221, (middle left) 222, (middle right) 223, (bottom left) 224, and (bottom right) 225, along with the temperature semidiurnal tidal phase profiles for August (black solid diamonds). The MILs can be seen in the second halves of nights 221 and 223.

and UT 06:00 between 90 km and 95 km. Although the averaged descending rate of this temperature maximum in night 221 seems to be close to diurnal tide vertical phase speed, such intensive temperature structure ($\Delta T > 30$ K) is unlikely to be solely induced by the weak diurnal tide during midlatitude summer time. This leads to our investigations of the inversion layers focusing on the second half of both night 221 (Figure 1, top right) and night 223 (Figure 1, middle right). To avoid confusion with semidiurnal tidal temperature features that were evident in the early evening, we only discuss the MIL structure starting from UT 07:55 on night 221.

It is also worth noting that the MIL-like temperature structure between UT 08:20 and UT 09:00 on night 223 is likely associated with an intensive mesospheric bore event, as observed by AMTM measurements during that night. Most of the necessary conditions used to identify a bore [*Dewan and Picard*, 1998; *Dewan and Rickard*, 2001] were fulfilled by this event: sharp front separating a dark (cold) and a bright (warm) regions, high phase speed of ~76 m/s, fixed pattern of trailing waves, their number increasing over time, and the inversion layer at the assumed altitude of the bore. However, further investigations would still be necessary to fully characterize this event. On the other hand, the lower temporal resolution of Na lidar measurements makes it difficult to distinguish the mesospheric bore from the inversion layer. Thus, we have focused on the time span UT 09:00 and UT 11:00 to study the MIL event observed on night 223.

Figure 1 also shows the differences between MIL events on nights 221 and 223. The MIL on 221 was nearly stationary until 8:45 UT when it abruptly began to propagate downward. In contrast, the MIL on night 223 showed no significant change in its peak altitude. In addition, the figure shows several extremely low temperature regions exhibiting compact spatial (a few kilometers wide) and temporal (less than 1 h) structures, with temperatures at or even below 150 K during each night of this campaign. The most notable cold spots occurred near 100 km around UT 06:00 on the night 218 (Figure 1, top left), two cold spots near 94 km and 92 km in the middle of night 223, and the one near 95 km near the end of night 224. Night 225 (Figure 1, bottom right) overall has much colder temperature than the other nights without obvious GW or tidal wave modulation behaviors but has sporadic cold spots throughout the night.

To diagnose the MIL structure and the associated wind variations in detail, Figure 2 focuses on the lidar temperature, zonal, and meridional wind profiles during these two events. The constant 200 K temperatures near the upper and lower limits of each profile replace data where the uncertainties are larger than 10 K. Similarly, winds at the end of zonal and meridional profiles are set to zero wind when the uncertainties are larger than 15 m/s. The figure shows that during the night of 221, the MIL was composed of two distinct segments. Before 08:45 UT, the layer (FWHM of ~5 km) exhibited no significant downward propagation near 90 km, with a peak temperature over 200 K. Thereafter, the layer started to propagate downward to ~85 km (by ~ 10:00 UT) with a speed of ~ 5 km/h, which is much faster than the diurnal tidal vertical phase speed, but close to typical semidiurnal tidal phase velocities. Although MIL events on both nights displayed similar magnitudes and widths, the MIL on night 223 was much more stable and maintained an altitude near 92.5 km throughout the event.

Meanwhile, the Thermosphere Ionosphere Mesosphere Energetics and Dynamics/Sounding of the Atmosphere using Broadband Emission Radiometry data for this night further revealed that this inversion layer was quite widespread and was observed to extend across the western USA and out over the Pacific Ocean, indicating its mesoscale nature. Figure 2 also shows that during the MIL events, the meridional wind and its vertical gradient experienced much larger variations than the zonal wind counterparts, which did not seem to be correlated with MILs.

### 3.1. Atmospheric Wind Shear and Instability During the MILs

Using the lidar temperature and wind data, we calculated the Brunt Väisälä frequency squared, $N^2$, as shown in the color contours of Figure 3a (night 221) and Figure 3b (night 223). (Note that the values of $N^2$ are multiplied by a factor of $10^4$ in both figures). The white areas indicate the vertical and temporal extent of convectively unstable regions, and the line contours on top of the color contours represent the horizontal wind shear during the inversions. Also, the altitudes where dynamic instability ($0 <$ Richardson Number ($Ri$) $< 0.25$) occurred are marked in both figures to provide a comprehensive spatial and temporal view of the atmospheric stability situation during the MILs. From the wind shear contours, the meridional wind shear exhibited larger oscillations than the zonal wind shear, consistent with our previous discussion of Figure 2. For example, Figure 3a shows that for night 221, the zonal wind gradient varied from near −12 m/s/km to 0 m/s/km between 85 km and 92 km where MIL occurred, while the meridional wind shear oscillated from −24 m/s/km to +24 m/s/km before

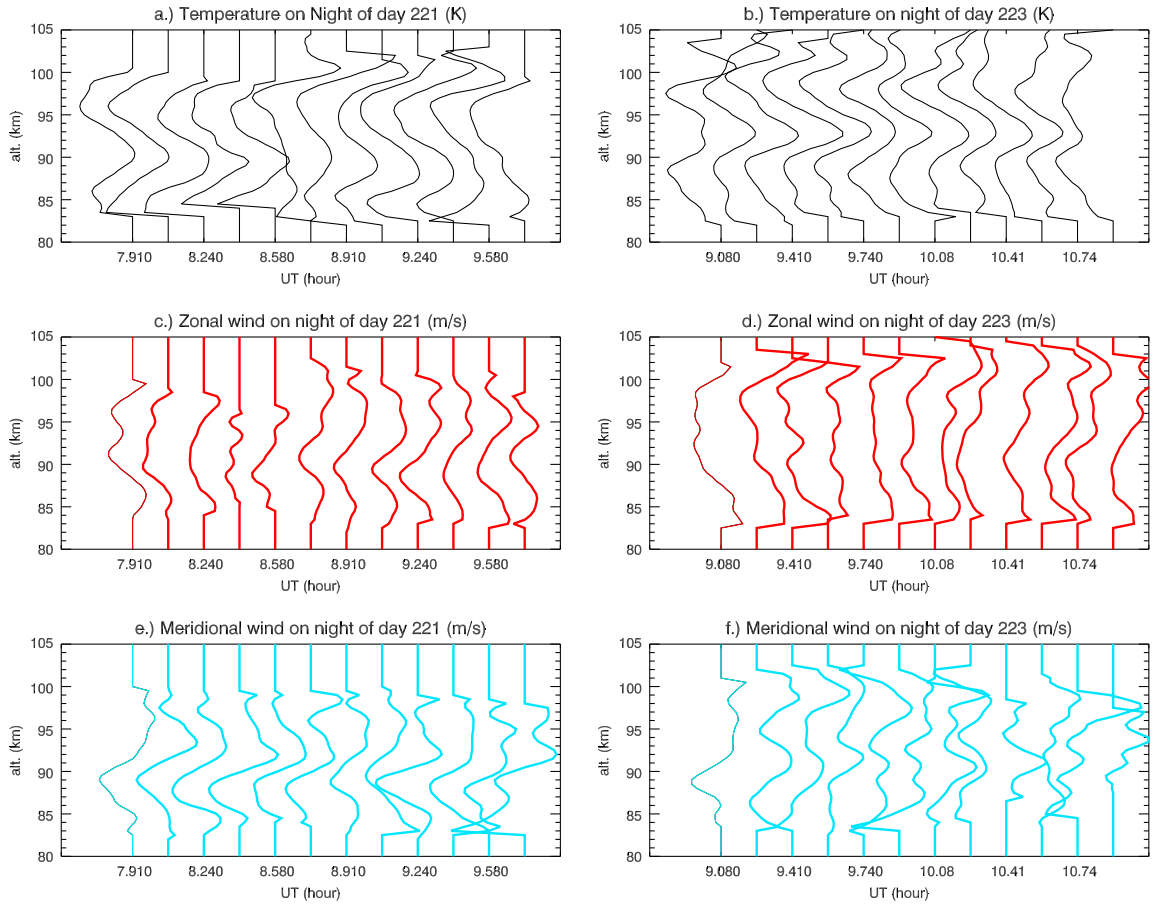


**Figure 2.** The lidar profiles of temperature (black), zonal wind (red), and meridional wind (light blue) during the MILs of (a, c, and e) night 221 and (b, d, and f) night 223.

it dropped back to near −12 m/s/km within the same altitude range. The scenario for the wind shear during night 223 was less vigorous; with similar zonal wind shear (between −12 m/s/km and 0 m/s/km) while the corresponding meridional wind varied from 12 m/s/km to −24 m/s/km. At the same time, several dynamic instability events occurred around the convectively unstable region (white) above the peak altitude of the MIL. This is expected since $Ri = N^2/S^2$, where $S$ is the horizontal wind shear, indicating that the region immediately above the MIL peak was highly unstable on both nights. Looking at both Figures 2a and 3a, this region is close to convectively unstable, where the vertical temperature gradient was ≤ the dry adiabatic lapse rate (−9.5 K/km in the mesopause region), and appears to have no significant downward propagation before 08:45 UT. Subsequently, this unstable layer, confined between two highly stable regions, expanded downward during the rest of the night. The disappearance of the lower (~91 km) stable region between 08:40 UT and 08:50 UT was coincident with the nonexistence of inversion structure in the temperature profile of 08:45 UT in Figure 2a, implicating a possible connection between the two features. The near convectively unstable region during night 223 remained near 89 km before 08:00 UT and then suddenly jumped to and stayed near 94–96 km from 08:30 UT onward. During this MIL, the convectively unstable region, also trapped between two highly stable layers, exhibited much larger vertical and temporal spans than that of night 221 and the instability events were less dynamic. Figures 2b and 3b also show an adiabatic/superadiabatic region parallel to and 2–3 km above the MIL on night 223.

On both of these occasions, these convectively unstable regions could have been generated by wave breaking-induced temperature gradient changes, which likely created further wave breaking when the subsequent GWs reached the unstable layers, and keeping them from propagating to higher altitude. Yet there are other possible schemes for this thermal and instability structure, which are discussed in section 3.2. Overall, the MIL events were highly correlated with the occurrence of convectively unstable

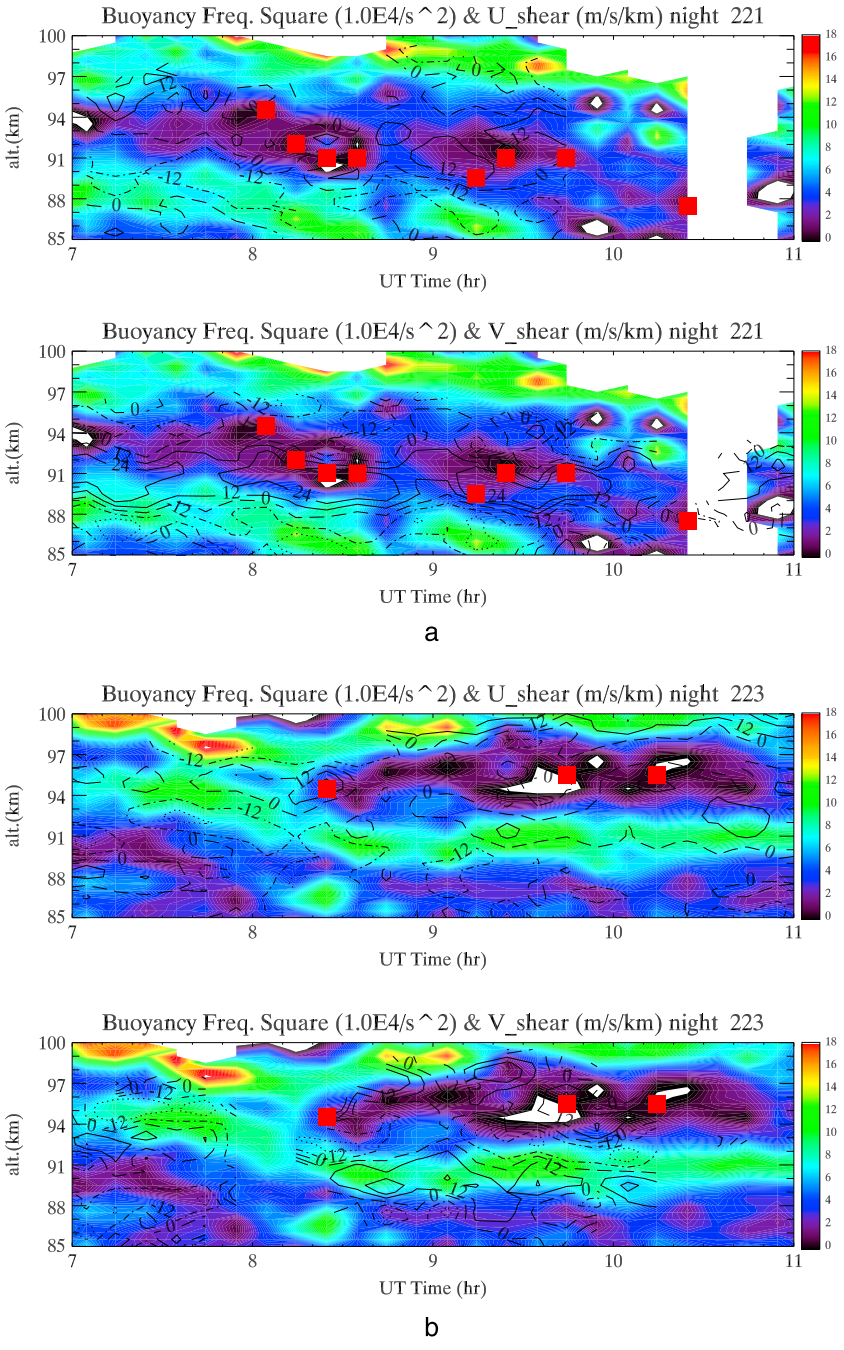


**Figure 3.** (a) Contour plots (color) of the lidar observed buoyance frequency square ($N^2$) during the second half of night 221. The values of $N^2$ have been multiplied by a factor of 1.0 E04. The line contour plots are the zonal (top) and meridional (bottom) wind shear with dotted line represents −24 m/s/km; dash-dotted line represents −12 m/s/km; long-dashed line represents the zero wind shear and solid line represents +12 m/s/km and larger wind gradient. And the red squares are altitudes of dynamic instability where $0 < Ri < 0.25$. (b) Same as Figure 3a, except for night 223.

regions, and both were sandwiched between two highly stable layers. During these events, strong wind shears and large variations in the meridional direction were observed near unstable regions.

### 3.2. GW Forcing and Zonal Wind Acceleration

The USU Na lidar's capability for GW zonal momentum flux (MF) measurements gives an extra parameter for this MIL study, by providing a direct view of the gravity wave forcing in the east-west direction within the

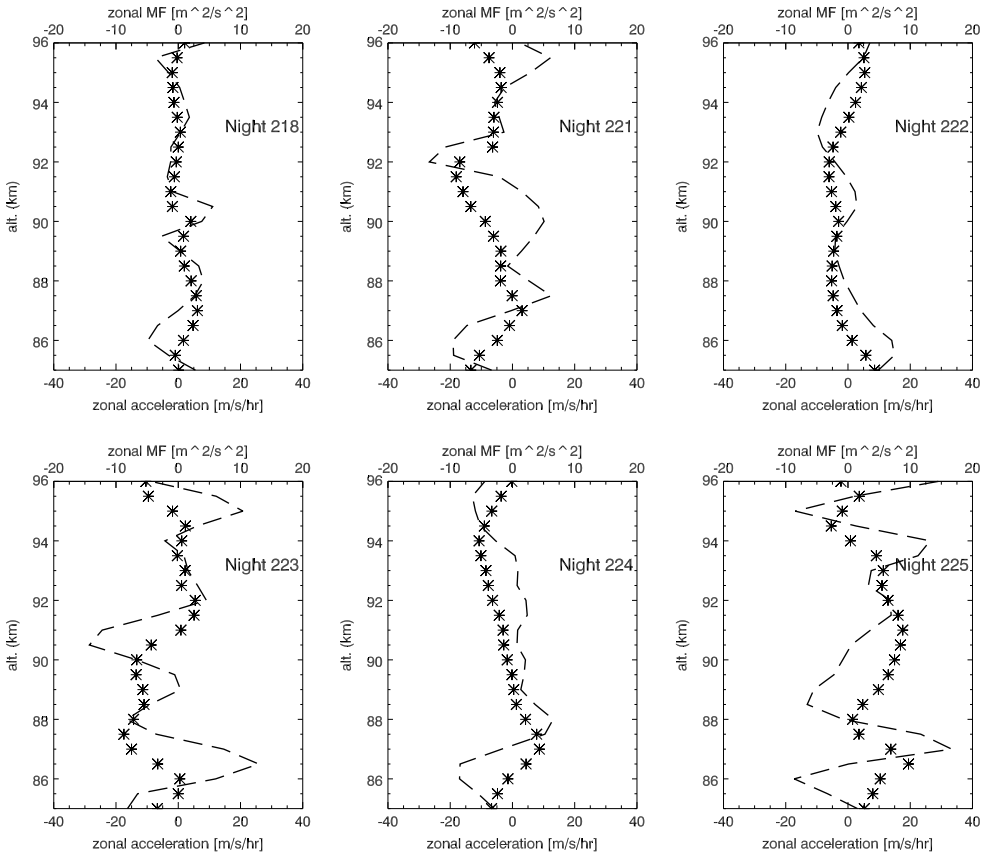


**Figure 4.** The lidar measurements of the GW-induced nightly averaged zonal momentum fluxes (asterisk) for the six nights, along with the deduced nightly averaged zonal wind accelerations (long-dashed lines). The top *x* axis represents the value range for momentum flux and the bottom *x* axis represents the value range for zonal wind acceleration.

mesopause region. The Na lidar MF measurement setup and algorithms for MF analysis are well documented in earlier literature [*Acott et al.*, 2011] and will not be reiterated in detail here. This measurement is based on the seminal study by *Vincent and Reid* [1983], who introduced the dual-beam technique and experimental designs in radar MLT measurement. In their study, the authors recognized that the velocity covariance $\overline{u'w'}$ can be estimated from the difference in radial velocity variances at two viewing angles, included at equal and opposite angles off-zenith in a vertical plane as $\overline{u'w'} = \left(\overline{\sigma_E^2} - \overline{\sigma_W^2}\right)/2\sin\theta$, where $\overline{\sigma_E^2}$ and $\overline{\sigma_W^2}$ are the spatial and temporal averaged velocity variances in beams inclined at an angle $\theta$ east and west from zenith. Figure 4 shows the nightly averaged zonal MF profiles (asterisks) deduced from the documented 2 h linear background subtraction (LBS) method [*Acott et al.*, 2011] during the six campaign nights within the altitude range of 85 to 96 km. The units for MF are $m^2/s^2$, and its range is labeled on the upper *x* axis extending from $-20\,m^2/s^2$ to $+20\,m^2/s^2$. According to linear saturation theory, the mean flow acceleration in the region where the monochromatic GW breaks is given by [*Holton*, 1982]

$$\left.\frac{\partial\overline{u}}{\partial t}\right|_{z=z_b} = -\frac{1}{\rho_0}\frac{\mathrm{d}}{\mathrm{d}z}\left(\rho_0\overline{u'w'}\right) = -\frac{1}{\rho_0}\frac{\mathrm{d}\rho_0}{\mathrm{d}z}\left(\overline{u'w'}\right) - \frac{\mathrm{d}\left(\overline{u'w'}\right)}{\mathrm{d}z} \tag{1}$$

Here $z_b$ is breaking altitude, and $\overline{u'w'}$ is the vertical flux of horizontal momentum. The USU Na lidar can measure the zonal momentum flux, $\overline{u'w'}$ during nighttime only where $u'$ and $w'$ are the perturbations of the horizontal and vertical winds, respectively, $\rho_0$ is air density at this altitude, and $\overline{u}$ is the horizontal wind projected in the wave propagation direction. Equation (1) shows that the mean flow acceleration depends on

the GW momentum flux and its vertical gradient. By assuming hydrostatic equilibrium within the mesopause region and applying ideal gas law, we have

$$\frac{1}{\rho_0}\frac{\mathrm{d}\rho_0}{\mathrm{d}z} = -\frac{1}{H} - \frac{1}{T_0}\frac{\mathrm{d}T_0}{\mathrm{d}z} \tag{2}$$

where $H$ is the scale-height and can be calculated using lidar temperature measurements. Therefore, equation (1) can be written as

$$\left.\frac{\partial \overline{u}}{\partial t}\right|_{z=z_b} = \left(\frac{1}{T_0}\frac{\mathrm{d}T_0}{\mathrm{d}z} + \frac{1}{H}\right)\left(\overline{u'w'}\right) - \frac{\mathrm{d}\left(\overline{u'w'}\right)}{\mathrm{d}z} \tag{3}$$

Since the Na lidar can measure all of these parameters in the mesopause region in the zonal direction, the nightly averaged zonal wind acceleration due to GW forcing can be directly deduced and is shown in Figure 4.

In order to obtain a sufficient S/N ratio for MF calculation, the lidar data were binned at 10 min intervals, thus enabling all perturbations with periods greater than 20 min to be resolved. The upper limit of the GW spectrum was 2 h for the MF results, due to the length of the LBS window. Therefore, the lidar MF represents mostly medium-scale GW forcing. From the figure, it is evident that the nightly averaged MF and MF gradients for 221 and 223 were larger than those on nights 218, 222, and 224. For example, during night 221, the MF in the altitude range of 95.5 km to 92.5 km ranged between 0 and $-3\ \mathrm{m^2/s^2}$, while near 91.5 km, it changed to $\sim -10\ \mathrm{m^2/s^2}$ and gradually reduced to near zero below 89 km. It then varied between $-5\ \mathrm{m^2/s^2}$ and $2\ \mathrm{m^2/s^2}$ below 87 km. For night 223, the significant MF occurred within the altitude range 86 km to 91 km, with values near $-10\ \mathrm{m^2/s^2}$. After staying close to zero between 91 and 94 km, the MF changed from $0\ \mathrm{m^2/s^2}$ to $-5\ \mathrm{m^2/s^2}$ at 96 km. Since the first term on the right-hand side of equation (3) is relatively small, due to insignificant value of its coefficient, the zonal wind acceleration heavily depends on the vertical gradient of MF. The two nights associated with MIL events show significant changes in GW-induced zonal wind accelerations, in contrast with nights 218, 222, and 224 which show much smaller wind accelerations. For the case of night 223, the zonal acceleration was $\sim -30$ m/s/h and +20 m/s/h near 90.5 km and 95 km, respectively, with another fast acceleration near 86.5 km of ~25 m/s/h. During night 221, the large zonal acceleration was found to be ~25 m/s/h and ~20 m/s/h near 92 km and 85.5 km, respectively.

Looking back at Figures 3a and 3b, it appears that the peak altitude of zonal acceleration was associated with the middle of the instability region above the highly stable layer, while peaks of acceleration near 86.5 km and 90.5 km during night 223, near 85.5 km during night 221 were most likely related to the other instability regions during the night that were outside of MIL events. For example, during the first half of night 223, there was another vertically confined near a convectively unstable region at 91 km between 04:00 UT and 07:00 UT, and a similar region was found on night 221 near 85 km between 04:00 UT and 06:00 UT. The case of night 225, when no apparent tidal feature was observed, is somewhat different. It had large GW forcing similar to that of night 223 near 87 km, and large oscillation with increasing altitude. The Lomb power spectrum density calculation for this night (not shown) indicates significantly more long period waves with periods between 40 min and 90 min as compared to the other five nights, so wave forcing due to these longer period, larger scale GWs may have contributed to this nightly MF.

## 4. Discussion

As this joint study of Na lidar and AMTM observations has shown so far, the MILs formation appears to be directly related to wave breaking-induced GW forcing. In addition, the lidar observations have revealed that each of the two intensive MILs (observed during night 221 and 223) were associated with convectively unstable region located above them and highly stable region below. We note that the lidar observed instability is a combination effect of the mean background instabilities and wave instabilities, which are difficult to separate. To better understand the dynamic scheme of these two events, it is important to review some theoretical studies regarding gravity wave breaking and instabilities in the middle and upper atmosphere.

It is believed, based on simple stability arguments [*Dunkerton*, 1984; *Fritts and Rastogi*, 1985], that convective instabilities should predominate for the breaking of high intrinsic frequency GWs, while dynamical instability

should predominate for the breaking of GWs close to the inertial frequency. A GW will also break upon reaching a critical level, when the horizontal wind matches its intrinsic horizontal phase velocity. Since most of the GWs in the MLT region propagate energy upward, the wave breaking process usually generates an upward flow that induces adiabatic cooling within the breaking region and a warming region below, due to increase of the downward heat flux of the process. The simultaneous deposition of energy and momentum through turbulence mixing affects the mean flow as well in the direction of propagation of the original GW. Modeling has shown that this cooling and warming process could be sufficient to generate a convectively unstable region that then prohibits subsequent GWs propagating above this altitude [*Liu and Hagan*, 1998]. Such a transition, with its vertical span close to GW's vertical wavelength, should happen on the order of a buoyancy period and a stable atmosphere should be restored fairly quickly. However, observations have shown this kind of convectively unstable layer occur frequently in the MLT region, especially around the mesopause. For example, *Williams et al.* [2002] describes a superadiabatic region that lasted several hours as observed by a sodium lidar. Long-lasting wave saturation, via local convective instability, may be due to wave superposition or wave-wave nonlinear interactions, especially parametric subharmonic instability that transfers energy from intermediate frequency GW to longer period secondary waves and can achieve local convective instability [*Thorpe*, 1994]. Yet the AMTM data in Table 1 do not reveal apparent harmonic periods in the GW spectrum during the two nights. *Fritts and Alexander* [2003, and references therein] have pointed out that Kelvin-Helmholtz (KH) instabilities, preferentially triggered by inertia-gravity waves could also form near-adiabatic layers sandwiched between temperature inversions. The lifetimes of the subsequent MILs can extend longer than those created by high-frequency wave breaking because of the time needed for the turbulence to expand throughout the whole shear layer. This projected feature resembles the thermal structure observed during the MIL events. Signs of inertia-gravity wave activity, however, were not observed during the two nights by either instrument. On the other hand, a strong diurnal tide could also trigger KH instability due to its relatively short vertical wavelength (~20 km in mesopause region). Large amplitude GW perturbations can change the mean temperature structure as well [*Vanzandt and Fritts*, 1989; *Fritts et al*., 2004], when enhanced GW dissipation and turbulent mixing occur in response to sharp increase in stability leading to wave amplification and enlarged temperature gradients.

We have already mentioned the numerical model studies on GW breakings on the presence of tidal wind [*Liu and Hagan*, 1998; *Liu et al*., 2000], which indicate that the superposition of the large tidal winds can enhance, and eventually push, a large wind shear downward due to its downward phase propagation. This process guides the GWs critical levels downward, forcing the subsequent GWs to break at lower altitude. The associated enhancement of downward heat flux during the wave breaking process continues to heat up the atmosphere below this altitude and forms a stable MIL that endures until the atmosphere restores its stability. This mechanism leads to the simultaneous downward propagation of the MIL, a feature that is consistent with the MIL observed during night 221 (after 08:55 UT), and with other reported events in the literature. Along with frequent dynamic instabilities between 88 km and 94 km, similar to the MIL structure during this period, the near convectively unstable region in the middle of the mesopause region between 07:00 UT and 09:00 UT on night 221 had no obvious (or a very slow) downward propagation. After 09:00 UT, the superimposition of the meridional semidiurnal tide and the changing mean flow due to GW breaking guided the critical levels of the northeast propagating GWs (listed in Table 1) downward, which drove the MIL to lower altitudes as well. The changing of the local thermal gradient during this process could alter the altitude of this near convectively unstable region, as shown in Figure 3a after 09:00 UT, and force subsequent GWs to saturate at lower altitudes, further strengthening the downward propagating MIL. However, this mechanism cannot explain the parallel MIL structure observed on night 223.

For the case of the intensive MIL during the second half of night 223, the situation was a bit more complex and quite different than on night 221. Since the onset of the convectively unstable or near unstable region accompanying the MIL near 08:35 UT, it was confined between two strong stable regions near 90 km and 99 km. The highly stable region near 99 km can be attributed to the large positive temperature gradient above the mesopause, which was near 97 km for both nights. It is intriguing to note that the onset of the MIL, with a near-adiabatic region above and highly stable region below, was almost at the same time as the arrival of an intensive mesospheric bore. It is well known that a "bore" event can quickly change the local temperature gradient [*Dewan and Picard*, 1998]. In this case, it was observed to increase the temperature by ~18 K within the altitude range of 90–93 km. This sudden change of the local thermal gradient, which lasted for the 40 min duration of the bore event (08:20 UT to 09:00 UT), is a good

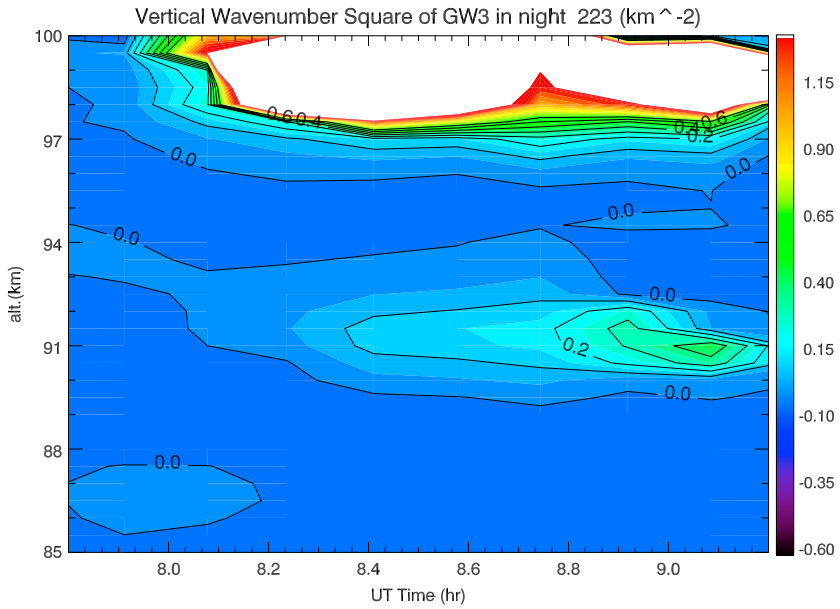


**Figure 5.** The variations of vertical wave number square ($m^2$) of the GW that was overlapping the time span of a mesospheric bore and the beginning of MIL of night 223. The 5.9 min period wave was propagating in the direction of 346° relative to the north with observed horizontal phase of 76 m/s.

candidate for generating the near convectively unstable region observed near 94 km and the enhanced buoyancy frequency near 90–91 km before 09:00 UT. Subsequently, the region between 93 km and 97 km became adiabatic, or superadiabatic, until 10:55 UT, creating conditions for increased wave breaking and turbulence generation.

Based on the enhanced saturation theory by *VanZandt and Fritts* [1989], the sharp increase of $N^2$ will locally induce enhanced turbulence and mixing above, accompanying an increase in the horizontal wind shear in the wave propagation direction. Additional effects also include heat flux convergence below the strong turbulence layer yielding further heating and enhanced positive temperature gradient, wave amplification, and instability, while heat flux divergence above the layer would reduce the mean temperature gradients at those altitudes [*Fritts et al*., 2004]. A GW will have its vertical scale (vertical wavelength) compressed as well, when it is propagating through this highly stable layer.

To study the above mentioned GW vertical scale variation during this process, we utilized the GW polarization relationship by *Hooke* [1986],

$$m^2 = \frac{N^2}{(c-u)^2} - k^2 - \frac{1}{4H^2} \tag{4}$$

where $m$ is vertical wave number and $k$ is horizontal wave number. Based on the hourly lidar horizontal wind and temperature measurements, coupled with AMTM measurements in Table 1, we have calculated the vertical wavelength of the observed small-scale GW within the OH layer during the second half of both nights from 08:00 UT to 11:00 UT. For example, Figure 5 shows the calculated $m^2$ of a 5.9 min GW propagating in the direction of 346° relative to the north with an observed horizontal phase speed of 76 m/s and horizontal wavelength of 27 km during its lifetime (07:50 UT to 09:10 UT) during night 223. This event was chosen because its lifetime overlapped with the mesospheric bore event and the beginning of the MIL and was least likely to encounter critical level filtering due to its high horizontal phase speed. It clearly shows the enhancement of $m^2$ (compression of vertical wavelength) within the altitude range of 89–93 km, corresponding to the bottom half of the MIL. The sudden and dramatic increase of $m^2$ above 97 km was most likely due to critical level formation. Other than these two confined regions, $m^2$ was close to zero over the rest of the mesopause region, indicating that the GW had a large vertical wavelength and its amplitude varied very little. This suggests that the mesospheric bore

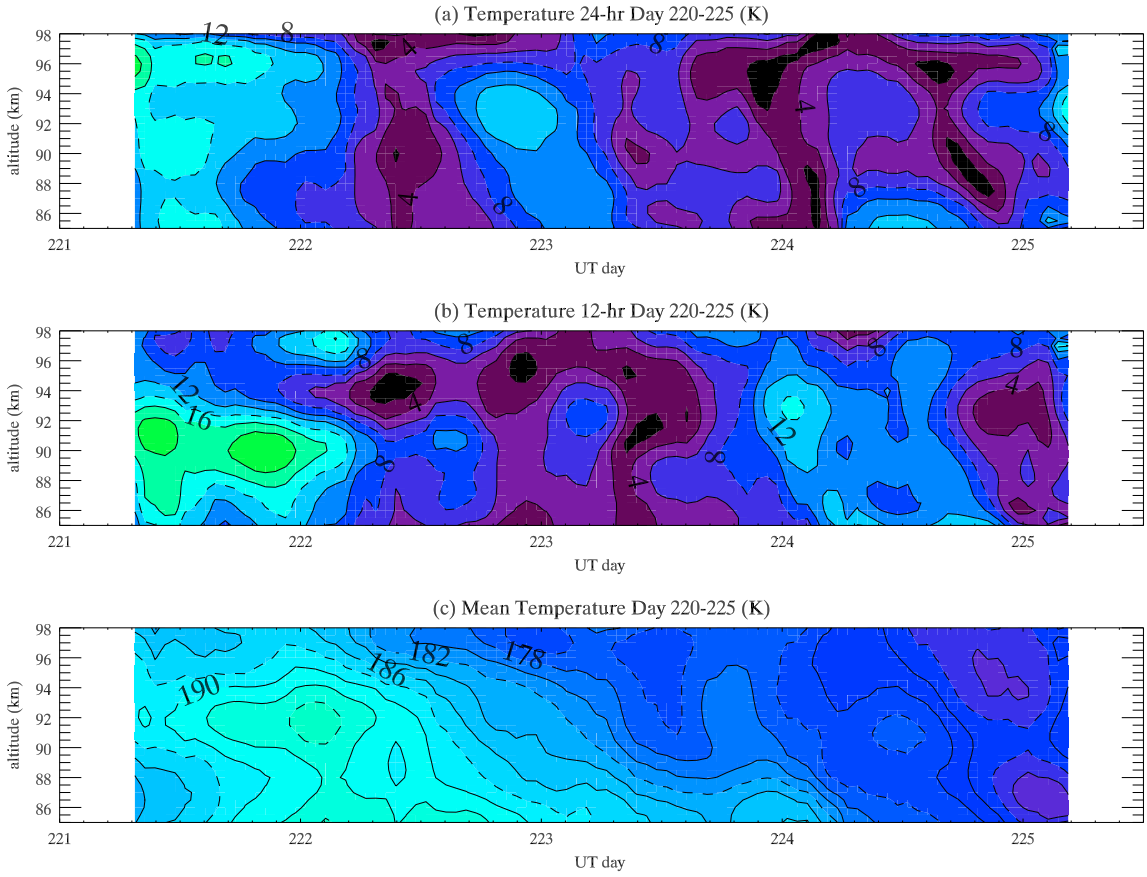


**Figure 6.** The variability of (a) diurnal, (b) semidiurnal temperature amplitude, and (c) the tidal removed mean temperature within the mesopause region during the lidar campaign.

induced a highly stable layer and compressed the vertical wavelength of a GW as it propagates through the layer. The scenario is consistent with the predictions of the enhanced saturation theory mentioned above, which also predicts the observed enhancement of convective and dynamic instability above the highly stable layer (as shown in Figures 3a and 3b).

The relationship between MIL and the stable layer can be further confirmed by closer inspection of both Figures 2a and 3a: the sudden changing of temperature gradient around 08:45 on night 221 removed the highly stable region temporarily and turned off the source for convergence of the downward heat flux, leading to the disappearance of the inversion layer. As described earlier, during the MIL event, the lidar observed a much larger increase in the wind shear in the meridional direction, which was the propagation direction of most of the GWs, than in the zonal direction. Again, this is consistent with the enhanced saturation theory, which predicts an increase of wind shear in the wave propagation direction. Figure 2 has also shown that the MIL peak altitude was 90 km in night 221 and 92.5 km for the case of 223, both with peak temperature near 210 K. The temperature drop from ~210 K near the MIL's peak altitude to the mesopause temperature (179.5 K for night 221 and 171 K for night 223) near 97 km generated a large negative temperature gradient and an associated adiabatic/superadiabatic region, between these two levels. Therefore, compared to night 221, the observed larger and longer unstable region during the MIL of night 223 was most likely due to the colder mesopause temperature and the higher altitude of the heating region, in addition to the increasing wave instability above the strong stable layer. The resulting prolonged superadiabatic region likely forced the high-frequency GWs to break nearby and subsequently formed the stable MIL for night 223.

Based upon the above discussion, the trigger that initiated the sharp increase in the buoyancy frequency (Figures 3a and 3b) becomes highly relevant to the formations of the two observed MILs.

While the sudden enhancement of the stability layers on night 223 could have been generated by the passage of an intensive mesospheric bore event as described earlier, the sudden increase in stability on night 221 could have been induced by a large amplitude long-period wave perturbation, such as a tidal wave. Indeed, both diurnal and semidiurnal temperature amplitudes during night 221 were the largest during the whole campaign based on the lidar temperature full diurnal cycle observations (Figure 6). For example, the semidiurnal tide between 90 and 92 km for day 221 had amplitude larger than 18 K, and larger than 12 K for the diurnal component during the second half of night. The slow downward propagation of the MIL before 09:00 UT suggests that the diurnal tide played a more important role than semidiurnal tide. The lidar meridional wind observations also show quite large diurnal tidal amplitude during night 221 ($>$30 m/s) near the peak altitude of MIL. The combination of the observed large meridional wind shear and the occurrence of strong dynamic instabilities (Figure 3a) may also suggest that this MIL structure could have been generated through diurnal tide-induced KH instability, instead of the previously described enhancement saturation scheme. In contrast, the diurnal and semidiurnal tidal temperature amplitudes were fairly small (~4–6 K) during the second half of night 223, excluding them from the formation of the highly stable layer that we have shown was related to the MIL that night. The tidal and mean temperature variability shown in Figure 6 were calculated with a 24 h sliding window at 1 h steps through the lidar measurements, while the harmonic fitting was conducted within the window to calculate the tidal period perturbations, including 24 h, 12 h, 8 h, and 6 h.

## 5. Summary and Conclusion

The study has investigated the occurrence of MILs within the mesopause region and their close association with breaking GWs as well as tidal-GW interactions, further enhancing our understanding of these temperature anomalies. Two strong MILs with intensity $\Delta T > 30$ K and FWHM of ~ 5 km were observed during a multiday coordinated campaign in early August 2011. The USU Na Lidar provided full diurnal cycle observations of temperature and horizontal wind, while the AMTM measured the nocturnal small-scale GW parameters. This campaign provided a unique opportunity for a comprehensive investigation of MIL formation and the associated atmospheric waves' characteristics (GWs and tidal waves), the atmospheric mean fields' condition and their variations during the MIL event. The results obtained from the simultaneous sets of Na lidar profiles of MLT winds and temperatures combined with the AMTM observations of horizontal temperature structures have demonstrated that the upper MIL formation process is likely dominated by GW wave breaking-induced forcing causing the downward transport of heat from a convectively unstable region to a region of high static stability.

Each event was associated with a convectively unstable region ~ 2–3 km above the peak of the MIL and a highly stable layer below it. On night 221, the MIL was observed to propagate downward during the second half of the event and behaved in a similar manner to previous MIL studies documented in the literature. On night 223, the MIL remained at an almost constant altitude, implying a different mechanic for its formation. The GW zonal momentum flux calculations during the campaign confirm that on the nights of the MILs strong wave forcing occurred in close proximity, ~1–2 km above each MIL. Although KH instability could have generated the inversion structure, the lidar revealed that the prolonged thermal and wind shear structure during the event support the enhanced saturation theory for their production [*VanZandt and Fritts*, 1989], which predicts the GW saturation process above a highly stable layer that heats up the region below the breaking region. The stable MIL in night 223 was likely formed by the prolonged convectively unstable layer formed by the above mechanism that forced the subsequent small-scale high-frequency GWs to break above the highly stable layer. These results were confirmed by lidar measurements of the atmospheric instability and momentum flux. Further investigation revealed that large tidal amplitudes were responsible for the sharp increase in the convective stability on night 221, while the enhanced stability layer during second half of night 223 was possibly triggered by the passage of a strong mesospheric bore event. This further demonstrates the importance of coordinated measurements to quantify dynamical processes and has revealed clear connections between local transient MIL anomalies and wave-driven dynamical variations in the upper atmosphere.

**Acknowledgments**
The USU Na lidar data have been promptly reorganized and uploaded to the newly established CRRL Madrigal database at http://madrigal.physics.colostate.edu/htdocs/. The lidar data for this study are available at this site. This study was performed as part of a collaborative research program supported under the Consortium of Resonance and Rayleigh Lidars (CRRL) National Science Foundation (NSF) grant 1135882, with additional support from NSF grants AGS-1041571 and AGS-0962544. The AMTM observations were supported by NSF grant AGS-1042227.

## References

Acott, P. E., C. Y. She, D. A. Krueger, Z. Yan, T. Yuan, J. Yue, and S. Harrell (2011), Observed nocturnal gravity wave variances and zonal momentum flux in midlatitude mesopause region over Fort Collins, Colorado, *J. Atmos. Sol. Terr. Phys.*, *73*, 449–456.

Cutler, L. J., R. L. Collins, K. Mizutani, and T. Itabe (2001), Rayleigh lidar observations of mesospheric inversion layers at Poker Flat, Alaska (65 N, 147 W), *Geophys. Res. Lett.*, *28*, 1467–1470.

Dao, P. D., R. Farley, X. Tao, and C. S. Gardner (1995), Lidar observations of the temperature profile between 25 and 103 km: Evidence of tidal perturbation, *Geophys. Res. Lett.*, *22*, 2825–2828.

Dewan, E. M., and R. H. Picard (1998), Mesospheric bores, *J. Geophys. Res.*, *103*, 6295–6305.

Dewan, E. M., and R. H. Rickard (2001), On the origin of mesospheric bore, *J. Geophys. Res.*, *106*, 2921–2927.

Duck, T. J., D. P. Sipler, and J. E. Salah (2001), Rayleigh lidar observations of a mesospheric inversion layer during night and day, *Geophys. Res. Lett.*, *28*, 3597–3600.

Dunkerton, T. J. (1984), Inertia-gravity waves in the stratosphere, *J. Atmos. Sci.*, *41*, 3396–3404.

Fritts, D. C., and M. J. Alexander (2003), Gravity wave dynamics and effects in the middle atmosphere, *Rev. Geophys.*, *41*(1), 1003, doi:10.1029/2001RG000106.

Fritts, D. C., and P. K. Rastogi (1985), Convective and dynamical instabilities due to gravity wave motions in the lower and middle atmosphere: Theory and observations, *Radio Sci.*, *20*, 1247–1277.

Fritts, D. C., B. P. Williams, C. Y. She, J. D. Vance, M. Rapp, F.-J. Lübken, A. Müllemann, F. J. Schmidlin, and R. A. Goldberg (2004), Observations of extreme temperature and wind gradients near the summer mesopause during the MaCWAVE/MIDAS rocket campaign, *Geophys. Res. Lett.*, *31*, L24S06, doi:10.1029/2003GL019389.

Hauchecorne, A., M. L. Chanin, and R. Wilson (1987), Mesospheric temperature inversion and gravity wave dynamics, *Geophys. Res. Lett.*, *14*, 935–939.

Holton, J. R. (1982), The role of gravity wave induced drag and diffusion in the momentum budget of the mesosphere, *J. Atmos. Sci.*, *39*, 791–799.

Hooke, W. H. (1986), Gravity waves, in *Mesoscale Meteorology and Forecasting*, edited by P. S. Ray, pp. 272–288, Am. Meteorol. Soc., Boston, Mass.

Huang, T. Y., H. Hur, T. F. Tuan, X. Li, E. M. Dewan, and R. H. Picard (1998), Sudden narrow temperature-inversion-layer formation in ALOHA-93 as a critical-layer-interaction phenomenon, *J. Geophys. Res.*, *103*, 6323–6332.

Liu, H.-L., and M. E. Hagan (1998), Local heating/cooling of the mesosphere due to gravity wave and tidal coupling, *Geophys. Res. Lett.*, *25*, 2941–2944.

Liu, H.-L., M. E. Hagan, and R. G. Roble (2000), Local mean state changes due to gravity wave breaking modulated by the diurnal tide, *J. Geophys. Res.*, *105*, 12,381–12,396.

Meriwether, J. W., and C. S. Gardner (2000), A review of the mesosphere inversion layer phenomenon, *J. Geophys. Res.*, *105*, 12,405–12,416.

Meriwether, J. W., and A. J. Gerrard (2004), Mesosphere inversion layers and stratosphere temperature enhancements, *Rev. Geophys.*, *42*, RG3003, doi:10.1029/2003RG000133.

Meriwether, J. W., and M. G. Mlynczak (1995), Is chemical heating a major cause of the mesosphere inversion layer?, *J. Geophys. Res.*, *100*, 1379–1387.

Meriwether, J. W., X. Gao, V. B. Wickwar, T. Wilkerson, K. Beissner, S. Collins, and M. E. Hagan (1998), Observed coupling of the mesosphere inversion layer to the thermal tidal structure, *Geophys. Res. Lett.*, *25*, 1479–1482.

Oberheide, J., H.-L. Liu, O. A. Gusev, and D. Offermann (2006), Mesospheric surf zone and temperature inversion layers in early November 1994, *J. Atmos. Sol. Terr. Phys.*, *68*, 1752–1763.

Sassi, F., R. R. Garcia, B. A. Boville, and H. Liu (2002), On temperature inversions and the mesospheric surf zone, *J. Geophys. Res.*, *107*(D19), 4380, doi:10.1029/2001JD001525.

She, C.-Y., et al. (2004), Tidal perturbations and variability in mesopause region over Fort Collins, CO (41 N, 105 W): Continuous multi-day temperature and wind lidar observations, *Geophys. Res. Lett.*, *31*, L24111, doi:10.1029/2004GL021165.

Sica, R. J., T. Thayaparan, P. S. Argall, A. T. Russell, and W. K. Hocking (2002), Modulation of upper mesospheric temperature inversions due to tidal-gravity wave interactions, *J. Atmos. Sol. Terr. Phys.*, *64*, 915–922.

Sica, R. J., P. S. Argall, T. G. Shepherd, and J. N. Koshyk (2007), Model-measurement comparison of mesospheric temperature inversions, and a simple theory for their occurrence, *Geophys. Res. Lett.*, *34*, L23806, doi:10.1029/2007GL030627.

States, R. J., and C. S. Gardner (2000), Thermal structure of the mesopause region (80–105 km) at 40 N latitude. Part II: Diurnal variations, *J. Atmos. Sci.*, *57*, 78–92.

Thorpe, S. A. (1994), Observations of parametric instability and breaking waves in an oscillating tilted tube, *J. Fluid Mech.*, *261*, 33–45.

VanZandt, T. E., and D. C. Fritts (1989), A theory of enhanced saturation of the gravity wave spectrum due to increases in atmospheric stability, *Pure Appl. Geophys.*, *130*, 399–420.

Vincent, R. A., and I. M. Reid (1983), HF Doppler measurements of mesospheric momentum fluxes, *J. Atmos. Sci.*, *40*, 1321–1333.

Williams, B. P., M. A. White, D. A. Krueger, and C. Y. She (2002), Observation of a large amplitude wave and inversion layer leading to convective instability in the mesopause region over Fort Collins, CO (41°N, 105°W), *Geophys. Res. Lett.*, *29*(17), 1850, doi:10.1029/2001GL014514.

Yuan, T., et al. (2006), Seasonal variation of diurnal perturbations in mesopause region temperature, zonal, and meridional winds above Fort Collins, Colorado (40.6°N, 105°W), *J. Geophys. Res. 111*, D06103, doi:10.1029/2004JD005486.

Yuan, T., H. Schmidt, C. Y. She, D. A. Krueger, and S. Reising (2008a), Seasonal variations of semidiurnal tidal perturbations in mesopause region temperature and zonal and meridional winds above Fort Collins, Colorado (40.6°N, 105.1°W), *J. Geophys. Res.*, *113*, D20103, doi:10.1029/2007JD009687.

Yuan, T., C.-Y. She, D. A. Krueger, F. Sassi, R. Garcia, R. G. Roble, H.-L. Liu, and H. Schmidt (2008b), Climatology of mesopause region temperature, zonal wind, and meridional wind over Fort Collins, Colorado (41°N, 105°W), and comparison with model simulations, *J. Geophys. Res.*, *113*, D03105, doi:10.1029/2007JD008697.

Yuan, T., C. Y. She, J. Forbes, X. Zhang, D. Krueger, and S. Reising (2010), A collaborative study on temperature diurnal tide in the midlatitude mesopause region (41°N, 105°W) with Na lidar and TIMED/SABER observations, *J. Atmos. Sol. Terr. Phys.*, *72*, 541–549.